Automatica 161 (2024) 111491

Contents lists available at ScienceDirect

Automatica

journal homepage: www.elsevier.com/locate/automatica

Multi-agent deployment in 3-D via reaction–diffusion system with radially-varying reaction ☆

Jing Zhang [a], Rafael Vazquez [b,*], Jie Qi [c,d], Miroslav Krstic [e]

[a] College of Information Engineering, Shanghai Maritime University, Shanghai 201306, China
[b] Department of Aerospace Engineering, Universidad de Sevilla, Camino de los Descubrimiento s.n., 41092 Sevilla, Spain
[c] College of Information Science and Technology, Donghua University, Shanghai 201620, China
[d] Engineering Research Center of Digitized Textile and Fashion Technology Ministry of Education, Donghua University, Shanghai, 201620, China
[e] Department of Mechanical and Aerospace Engineering, University of California San Diego, La Jolla, CA 92093-0411, USA

ARTICLE INFO

Article history:
Received 24 July 2022
Received in revised form 16 September 2023
Accepted 22 December 2023
Available online xxxx

Keywords:
Backstepping
Boundary control
Radially-varying coefficient
Singular equations
Multi-agent system
Deployment

ABSTRACT

This paper considers the problem of the deployment of a set of agents distributed on a disk-shaped grid onto three-dimensional (3-D) profiles, by using a continuum approximation (valid in the limit for a large number of agents) and then a control methodology for partial differential equations (PDEs). The agents' collective behavior is modeled by a pair of radially-varying diffusion–reaction PDEs in polar coordinates, whose state determines the agents' position. Having a radially-varying reaction coefficient not only increases the challenge of kernel equations becoming singular in radius, but also brings more potential deployment manifolds. To stabilize and increase the convergence of the deployment, a boundary controller and a boundary observer are designed by combining an infinite-dimensional backstepping approach with a Fourier series decomposition technique, thus driving all agents to the desired profile. A key feature of the presented result is that the desired profile only needs to be known by the leaders, with the followers only needing to follow a simple control strategy which requires only the measurement of its current position and communication with its neighbors as defined by the multi-agent system topology. The method provides closed-loop exponential stability with any prescribed convergence rate in the L^2 norm. Simulation tests are shown to prove the effectiveness of the proposed algorithm.

1. Introduction

Large-scale collective behavior, such as complex animal groups, or even non-living systems involving physical–chemical interactions, is a pervasive phenomenon in nature (Vicsek & Zafeiris, 2012). Inspired by natural collective behaviors, research on multi-agent systems (MASs) has drawn significant attention from control scientists. Cooperative control of MASs was usually treated using ordinary differential equations (ODEs) models in most of existing studies, in which each agent's behavior is described by an ODE (Oh et al., 2015). Graph theory (Zheng et al., 2019), matrix theory (Chen et al., 2015; Hua et al., 2016), or potential functions (Gazi, 2005; Zavlanos et al., 2009) have been widely applied, to these models, and have already produced an impressive array of results.

More recent work have dramatically expanded the scale of these multi-agent systems (Bandyopadhyay et al., 2017; Chung et al., 2018; Rubenstein et al., 2014). With the explosion of the system scale, the limitation of ODE-based modeling gradually is revealed. As the number of agents increases, it is hard to add control inputs to every node. Thus, a novel continuum-based perspective is taken more attention, and a number of recent works focus on MASs with partial differential equation (PDE) models. The Laplacian operator in the heat equation over the graph has similar behavior to the Laplacian control for state consensus, as the result of the discrete and continuous approaches being essentially equivalent (Ferrari-Trecate et al., 2006). The approximation error between the PDEs and its corresponding discretized system is studied in Hao and Barooah (2012), which demonstrates that the Laplacian consensus dynamics can be formulated as a

☆ This work was supported by the National Natural Science Foundation of China (62173084, 61773112), the Project of Science and Technology Commission of Shanghai Municipality, China (23ZR1401800, 22JC1401403). Rafael Vazquez acknowledges support by grant TED2021-132099B-C33 funded by MCIN/ AEI/ 10.13039/501100011033 and by "European Union NextGenerationEU/PRTR." The material in this paper was not presented at any conference. This paper was recommended for publication in revised form by Associate Editor Andrea Cristofaro under the direction of Editor Sophie Tarbouriech.

* Corresponding author.
E-mail addresses: zhang.jing@shmtu.edu.cn (J. Zhang), rvazquez1@us.es (R. Vazquez), jieqi@dhu.edu.cn (J. Qi), krstic@ucsd.edu (M. Krstic).

https://doi.org/10.1016/j.automatica.2023.111491

linear PDE. The underlying communication topology connecting different agents is imposed by the spatial domain and selected discretization scheme. The application of the finite difference method transforms the spatial derivative of PDEs into the connection between the agent and its neighbors (Frihauf & Krstic, 2010). With the PDE approach, the contamination of the model by various quantities, most notably the number of agents and the agent indexing, which introduce a "microscopic distraction" into the study of a large collective, is postponed until the discrete implementation stage, rather than allowing the contamination in the design process.

Here, we review some related work using PDE models. Fu et al. (2019) construct an appropriate Lyapunov function to addresses containment control problem of multi-agent coordination governed by the heat equation and the wave equation. Output consensus without and with input constraint is studied in Yang et al. (2018) with boundary control, with dynamics modeled as parabolic PDEs. Pilloni et al. (2015) propose a nonlinear sliding-mode based consensus protocol to address the problem of driving the state of a network of identical agents towards a common steady-state profile, using a heat equation, with persistent disturbances at boundary. In order to achieve a desired density distribution in 1-D and 2-D, Krishnan and Martínez (2018) design the distributed control law for the spatial self-organization swarm using a Navier–Stokes model. In addition to consensus, the view of PDE-based modeling for MASs have been employed for deployment (Qi, Tang et al., 2019; Wei et al., 2019), time-varying formations (Qi et al., 2017; Zhao et al., 2018), motion planning (Freudenthaler & Meurer, 2020; Meurer & Krstic, 2011), inputs with time-delay (Qi, Wang et al., 2019; Selivanov & Fridman, 2022; Terushkin & Fridman, 2021), formation tracking (Tang et al., 2017) and sensor networks (Wu & Wang, 2015). Moreover, the backstepping method is a promising option to easily obtain boundary control, which has worked well for numerous PDE-based problems (Auriol, 2020; Koga et al., 2020; Zhang & Qi, 2021; Zhang et al., 2022).

This paper applies and extends our n-dimensional design of Vazquez et al. (2023) for deployment of multi-agents onto 3-D manifolds using two diffusion–reaction PDEs with spatially varying coefficients, following the ideas of Qi et al. (2015). Compared with the previous relevant results, the contributions of this paper are threefold.

First of all, based on the ideas of Qi et al. (2015), we design control protocol to drive agents to desired profile governed by the nonzero equilibrium of a PDE model. The PDE model is equivalent to the corresponding ODE model up to a second-order error, and the partial derivatives in space of the PDE reflect the relationship between neighbors' ODE models. The follower's control protocol corresponds directly to the PDE model, however a majority of profiles are unstable. Stabilization is ensured by leaders, located at boundary of the topology, which are required as boundary conditions for the PDE model. The leader's control protocol is designed utilizing the backstepping method, which has been found a wide application in boundary control designs, not only for Cartesian coordinate system, but also in polar or spherical coordinates, such as rings, disks, or even n-balls. Combining the backstepping method and spherical harmonics, Vazquez and Krstic (2016b) proposed an output-feedback controller to stabilize the reaction–diffusion equation on the n-ball, which was the basis of Qi et al. (2015), but only for constant coefficients; the extension to spatially-varying coefficients is challenging and has only recently been tackled (see Vazquez et al. (2023)), but allows for a much wider array of deployment profiles. Other existing related results cannot address such profiles, since they are mostly in one-dimensional spaces or assume symmetry conditions to reduce the difficulty (Deutscher & Kerschbaum, 2018; Li & Xie, 2010; Vazquez & Krstic, 2016a, 2019), even though some of the ideas were already presented in Vazquez et al. (2019), where the backstepping method is combined with a Fourier series approach to obtain an exponential stability result with prescribed convergence rate.

In addition, in order to significantly reduce communication costs, we design an observer by the backstepping approach, which is employed in the feedback law. The observer only needs to have the information of leader group and the nearest neighbors to estimate the positions of all agents. Combining the PDE models, controller and observer and discretizing, an output feedback control protocol is finally proposed for leaders and followers, in which all the agents require only local information and desired deployment is only known to the leaders. In addition, the exponential stability in L^2 norm for the MAS with a boundary sensor is proven. It must be emphasized that the designs of Qi et al. (2015) would not be of application, due to the radially-dependent coefficients.

Finally, the key idea of the backstepping method is to find an integral transformation to map the unstable original system to a stable target system to ensure the stability of the closed-loop system. To find this transformation, a kernel equation needs to be solved, which is not so straightforward when processing the radially-varying reaction–diffusion model (in the constant-coefficient case, the kernels were explicit). A numerical scheme by power series replacement is utilized, which greatly facilitates the solution process of the kernel; this approach has been proved convergent in Vazquez et al. (2023). Finally, simulation examples show that the method is effective for deployment as well as smooth evolution between different manifolds.

The paper is organized as follows. Section 2 describes the leader-actuated deployment model of multi-agents in 3-D space. Design method of boundary actuator and sensor are explained in Sections 3 and 4, respectively, while the stability of the output feedback system is analyzed. Section 5 connects the continuous PDE model with the agents' discrete control protocol again. A numerical scheme is discussed in Section 6 that provides a simpler method to calculate the kernels. Then results of deployment simulation are presented. Conclusions are summarized in Section 7.

2. Multi-agent model in 3-D

2.1. From discrete model to continuum model

In this paper, we consider the 3-D deployment problem comprising $M \times N$ agents indexed by $(i, j) \in \mathcal{I}$, where $\mathcal{I} = \{(i, j) : i = 1, 2, \ldots, M; j = 1, 2, \ldots, N\}$, with $M, N \in \mathbb{N}^+$. The information interaction between agents is given by the mesh-grid disk 2-D communication topology shown in Fig. 1. (i, j) denotes an agent located at the ith ray layer and the jth angle layer. An undirected graph $\mathcal{G} = (\mathcal{V}, \mathcal{E})$ consists of the set of nodes $\mathcal{V} = \{1, 2, \ldots, M \times N\}$ representing agents and $\mathcal{E}$ is the set of edges of graph. If $\big((i, j), (i', j')\big) \in \mathcal{E}$, then (i, j) and (i', j') are neighbors. Let $\mathcal{N}_{ij} = \{(i', j') : \big((i, j), (i', j')\big) \in \mathcal{E}\}$ denotes all neighbors of agent (i, j), thus all communication interaction between any agent (i, j) and its neighbors $\mathcal{N}_{ij}$ is described by the edges $\mathcal{E}$.

Note that the neighbors here represent neighbors on the topological structure, not on the physical space. The yellow node at the outermost layer denotes a leader, i.e., $i = M, j = 1, \ldots, N$, which has one follower neighbor and $N - 1$ leader neighbors; the blue node denotes a follower. The innermost layer followers have three neighbors and the rest have four. Let $(x_{ij}^1(t), x_{ij}^2(t), x_{ij}^3(t))$ denote the position of agent (i, j) at time t in 3-D. A simple

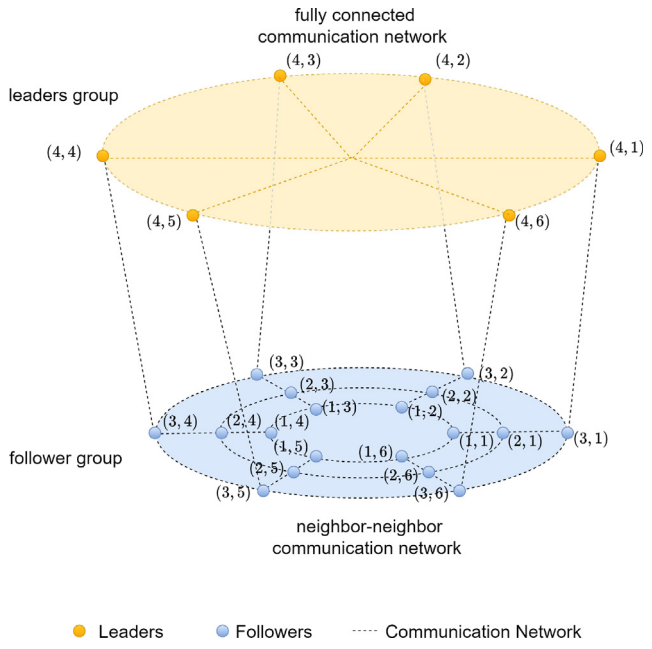

Fig. 1. A schematic diagram of an interaction topology with 4×6 agents. The yellow points represent the leaders (located at the outermost layer), and the blue ones are the followers. The dashed line represents the communication network, that is, any two agents connected by a dashed line are neighbors and can communicate with each other. For example, the agent indexed by $(2, 6)$ has four neighbors, namely $(2, 5)$ and $(2, 1)$ in the second layer and $(1, 6)$ and $(3, 6)$ in the radial direction. (For interpretation of the references to color in this figure legend, the reader is referred to the web version of this article.)

consensus protocol for each follower can be generally expressed by a set of ODEs, as follows

$$\dot{x}_{ij}^k(t) = \sum_{(i',j')\in\mathcal{N}_{ij}} \alpha_{i'j'}^{kij}(x_{ij}^k(t) - x_{i'j'}^k(t)) + \beta^{kij}x_{ij}^k(t), \tag{1}$$

where $k = 1, 2, 3$, and $\alpha_{i'j'}^{kij}$ β^{kij} denote weighting factors. The above followers' protocols only utilize the local information from itself and its neighbors to achieve consensus. In order to deploy all agents to the desired profile, the control signals to be designed are applied to leaders $i = M$, $j = 1, \ldots, N$, as follows

$$x_{Mj}^k(t) = u_j^k(t), \tag{2}$$

where $u_j^k(t)$ is the control input to be designed in the k direction for the leader agent (M, j). The leaders know the desired profile and drive all agents by exchanging information with the leader group and its follower neighbors.

Following Ferrari-Trecate et al. (2006), a multi-agent system composed of a large number ODEs can be represented by a continuous PDE, which has the same dynamics as the consensus control, as the spatial derivatives of the PDE model capture the relationship between neighbors. Thus, when M and N are large enough, the discrete ODEs-based model (1)–(2) is well-approximated by a continuum model as follows. First, the communication graph $\mathcal{G}$ is identified with a closed disk domain $\mathcal{D} = \{(r, \theta) : r \in [0, R], \theta \in [0, 2\pi)\}$ by defining, for (i, j), a grid covering the disk. One easy example would be $(r_i, \theta_j) = \left(\frac{R}{M}i, \frac{2\pi}{N}j\right)$ (see Section 5 for the grid actually used in the implementation, which is slightly more complex). Let $v(t, r_i, \theta_j) = x_{ij}^1(t) + \mathrm{i}x_{ij}^2(t)$ be complex-valued and $z(t, r_i, \theta_i) = x_{ij}^3$ be real-valued. Similarly for the leaders, $v(t, R, \theta_j) = u_j^1(t) + \mathrm{i}u_j^2(t)$ and $z(t, R, \theta_j) = u_j^3(t)$. Now consider a large number of agents so that one can consider that $M \to \infty, N \to \infty$ and then one can approximate $(r_i, \theta_j) \to (r, \theta)$. Thus, v and z become continuous variables in r and θ. Therefore, $(v(t, r, \theta), z(t, r, \theta))$ denotes the horizontal and vertical coordinates of the agent indexed by (r, θ) at time t in 3-D space and in particular $(v(t, R, \theta), z(t, R, \theta))$ the horizontal and vertical coordinates of the leader indexed by θ. Adequately choosing the consensus protocol of (1) (see Section 5 for details), the collective dynamics is then modeled by two diffusion–reaction equations, which evolve in polar coordinates (r, θ), as follows

$$v_t = \frac{\varepsilon}{r}(rv_r(t, r, \theta))_r + \frac{\varepsilon v_{\theta\theta}(t, r, \theta)}{r^2} + \lambda(r)v(t, r, \theta), \tag{3}$$

$$z_t = \frac{\gamma}{r}(rz_r(t, r, \theta))_r + \frac{\gamma z_{\theta\theta}(t, r, \theta)}{r^2} + \mu(r)z(t, r, \theta), \tag{4}$$

for $(t, r, \theta) \in \mathbb{R}^+ \times \mathcal{D}$. The radially-varying reaction coefficients are bounded, and the bounds are $\bar{\lambda} = \max_{r\in[0,R]} |\lambda(r)|$, $\bar{\mu} = \max_{r\in[0,R]} |\mu(r)|$. Here, the subscripts $v_t(t, r, \theta) = \partial v/\partial t$, $v_r(t, r, \theta) = \partial v/\partial r$ and $v_{\theta\theta}(t, r, \theta) = \partial^2 v/\partial\theta^2$ are the compact form of partial derivatives of v in the respective variable. The parameters ε and γ are the diffusion coefficients, which capture diffusion velocity, thus influencing the speed at which the agent converges to the desired profile. On the other hand the parameters λ and μ are reaction coefficients, which help generate more potential formations. The Laplacian operator in polar coordinates, given by the first two terms on right-hand side of (3) and (4), has the same effect as consensus control. Note that the followers' velocity-actuated feedback control laws are obtained by the right-hand side of (3) and (4).

Assumption 1. Assume that the system (3)–(4) satisfies the following conditions: $v, \varepsilon \in \mathbb{C}$, $z, \gamma \in \mathbb{R}$, and radially-varying reaction coefficients $\lambda(r)$, $\mu(r)$ are even analytic functions on $r \in [0, R]$.

A control protocol is proposed for the leaders implying the following boundary conditions for (3)–(4)

$$v(t, R, \theta) = \bar{v}(R, \theta) + V(t, \theta), \tag{5}$$

$$z(t, R, \theta) = \bar{z}(R, \theta) + Z(t, \theta), \tag{6}$$

where $\bar{v} \in \mathbb{C}$, $\bar{z} \in \mathbb{R}$ describe the desired profile that the agents should follow. Note that this is the continuum version of (2), decomposed in horizontal (5) and vertical (6) components. The open-loop system is not stable if the minimum value of the real parts of λ and μ are large enough, thus $V(t, \theta)$, $Z(t, \theta)$ need to be designed to actuate the multi-agent system. (5) and (6) serve as the boundary conditions for (3) and (4), thus how to deploy a discrete multi-agent system becomes how to control a continuous PDEs. In the sequel, we omit the arguments (t, r, θ) to save space.

2.2. Desired deployment profiles

The desired deployment profile $\{\bar{v}(r, \theta), \bar{z}(r, \theta)\}$ satisfies the following equilibrium equations:

$$\frac{\varepsilon}{r}(r\bar{v}_r)_r + \frac{\varepsilon}{r^2}\bar{v}_{\theta\theta} + \lambda(r)\bar{v} = 0, \tag{7}$$

$$\frac{\gamma}{r}(r\bar{z}_r)_r + \frac{\gamma}{r^2}\bar{z}_{\theta\theta} + \mu(r)\bar{z} = 0, \tag{8}$$

with the boundary conditions

$$\bar{v}(R, \theta) = f(\theta), \tag{9}$$

$$\bar{z}(R, \theta) = g(\theta), \tag{10}$$

where $f(\theta), g(\theta) \in \mathcal{C}^1([-\pi, \pi])$, $\bar{v}(r, \theta) = x(r, \theta) + \mathrm{i}y(r, \theta)$, and $\{x, y, z\}$ denotes the horizontal and vertical coordinates of agent in 3-D space. By setting different parameter sets $\{\varepsilon, \gamma, \lambda, \mu, f, g\}$ with $\lambda(r)$ and $\mu(r)$ radially-varying, one can obtain a wide range of interesting deployment profiles (not possible with constant λ

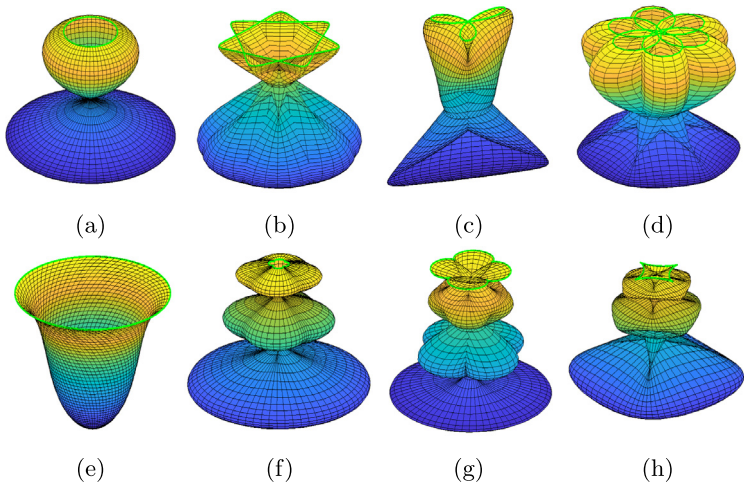

Fig. 2. Agent deployment profiles with $\varepsilon = \gamma = 1$. The first line with $\lambda(r) = 40 - 20\cos(\pi r)$, $\mu(r) = 50r^2$. Boundary conditions are (a) $f = e^{i\theta}$, $g = 1$, (b) $f = e^{2i\theta} + (1/5)e^{-5i\theta}$, $g = 1$, (c) $f = e^{i\theta} + e^{-2i\theta}$, $g = 1$, (d) $f = e^{i\theta} + e^{-5i\theta}$, $g = 1$. The parameters of deployment profiles for the second line are (e) $\lambda(r) = 10e^{2ir}$, $\mu(r) = 10$, $f = 200(e^{i\theta})$, $g = 100$, (f) $\lambda(r) = 200r$, $\mu(r) = 10$. $f = 200e^{1i\theta} - (1/5)e^{5i\theta}$, $g = 100$, (g) $\lambda(r) = 145\cos(1/4\pi r)$, $\mu(r) = 12$, $f = 200e^{i\theta} - (1/5)e^{5i\theta}$, $g = 2$, (h) $\lambda(r) = 240r$, $\mu(r) = 15\cos(2\pi r - 1/2\pi)$, $f = 200e^{i\theta} - (1/3)e^{-3i\theta}$, $g = 100$.

and μ). Some examples are given in Fig. 2. Note that the four profiles in the first line of Fig. 2 use the same value of $\lambda(r)$ and $\mu(r)$, only the leaders' configuration is different. The profiles of the second line employ different values of $\lambda(r)$ and $\mu(r)$. Obviously, with the increase of $\lambda(r)$ and $\mu(r)$, the deployment profiles present more possibilities in the longitudinal direction.

Remark 1. Under Assumption 1, there exists a unique solution $\bar{v}(r,\theta) \in \mathbb{C}$, $\bar{z}(r,\theta) \in \mathbb{R}$ for (7)–(10).

3. Boundary control design

Since v and z are independent of each other, and z is a special case of v, we only analyze the v-system in detail to save space. For the z-system, it easily get the result from v. Before designing the control, we first define the error variable $u(t,r,\theta) = v(t,r,\theta) - \bar{v}(r,\theta)$ between the actual position and the desired position. Then, the dynamics of error system is given by

$$u_t(r,\theta,t) = \varepsilon\frac{(ru_r)_r}{r} + \varepsilon\frac{u_{\theta\theta}}{r^2} + \lambda(r)u, \tag{11}$$

$$u(t,R,\theta) = U(t,\theta). \tag{12}$$

Here, the variable $U(t,\theta)$ is the control to be determined, which ensure that the error converges to zero, so that the agents can be driven to the desired position. Then, we combine the theory of Fourier series with the backstepping method to design the control.

3.1. Dimension reduction by Fourier series

Using a Fourier series to expand the system (11) and the boundary control (12), we have

$$u(t,r,\theta) = \sum_{n=-\infty}^{n=\infty} u_n(t,r)e^{in\theta}, \tag{13}$$

$$U(t,\theta) = \sum_{n=-\infty}^{n=\infty} U_n(t)e^{in\theta}, \tag{14}$$

where the coefficients (sometimes referred to as "modes") are defined as

$$u_n(t,r) = \frac{1}{2\pi}\int_{-\pi}^{\pi} u(t,r,\psi)e^{-in\psi}\,d\psi, \tag{15}$$

$$U_n(t) = \frac{1}{2\pi}\int_{-\pi}^{\pi} U(t,\psi)e^{-in\psi}\,d\psi, \tag{16}$$

we obtain that each coefficient u_n for all $n \in \mathbb{Z}$ satisfies the following 1-D reaction–diffusion equation (without angle dependency):

$$u_{nt}(t,r) = \frac{\varepsilon}{r}(ru_{nr})_r - \frac{\varepsilon n^2}{r^2}u_n + \lambda(r)u_n, \tag{17}$$

$$u_n(t,R) = U_n(t). \tag{18}$$

Result of the Fourier series, the different modes are independent of each other and can be analyzed separately.

3.2. Open-loop stability properties in Fourier space

We note that large modes without control are exponential stable as expected, so only a limited number of modes need to be stabilized. Next we analyze the stability properties for large modes. Before stating the stability of open-loop system, first we give an inequality and we introduce a definition that will be used later. The Poincare's inequality for u_n is

$$\int_0^R |u_n|^2 r\,dr \le 4R^2\int_0^R |u_{nr}|^2 r\,dr. \tag{19}$$

Definition 1. The L^2 norm $\|\cdot\|_{L^2}$ in polar coordinates is

$$\|f\|_{L^2}^2 = \int_0^R |f(r)|^2 r\,dr, \tag{20}$$

where $|f|^2 = ff^*$, being f^* the complex conjugate of f.

Lemma 1. *There exists $\bar{N} \in \mathbb{N}$ such that, for all $|n| > \bar{N}$, the equilibrium u_n of system (17)–(18) is open loop exponentially stable, i.e., for $U_n = 0$ in (18) there exists a positive constant D such that*

$$\|u_n(t,\cdot)\|_{L^2}^2 \le e^{-Dt}\|u_n(0,\cdot)\|_{L^2}^2, \tag{21}$$

where D is independent of n.

Proof. To prove the stability, a Lyapunov function is defined as

$$V_1(t) = \frac{1}{2}\|u_n(t,r)\|_{L^2}^2 \tag{22}$$

Taking the derivative of the Lyapunov function and using the inequality (19), we thus get that

$$\begin{aligned}\dot{V}_1 &= \int_0^R \frac{u_n^* u_{nt} + u_n u_{nt}^*}{2}\,\mathrm{d}r \\ &\le -\frac{\varepsilon_R}{4R^2}\int_0^R |u_n|^2 r\,\mathrm{d}r - \int_0^R \left(\frac{n^2\varepsilon_R}{r^2} - \lambda(r)\right)|u_n|^2 r\,\mathrm{d}r \\ &\le -\left(\frac{\varepsilon_R + 4n^2\varepsilon_R}{2R^2} - 2\bar{\lambda}\right)V_1, \end{aligned} \tag{23}$$

where ε_R is the real part of ε. Then taking $\bar{N} \in \mathbb{N}$, such that

$$\bar{N} \ge \sqrt{\frac{R^2(D+2\bar{\lambda})}{2\varepsilon_R} - \frac{1}{4}}. \tag{24}$$

Obviously, we get for all $|n| \ge \bar{N}$, that $\dot{V}_1 \le -DV_1$. Thus the lemma has been proven.

3.3. Stabilization of unstable modes

This part is mainly to design boundary control to stabilize the unstable mode with $|n| < \bar{N}$. Since the different modes are not coupled, it allows us to stabilize them separately and re-assembling them. Based on the backstepping (Krstic & Smyshlyaev, 2008) method, our idea is utilizing a invertible Volterra integral transformation

$$w_n(t,r) = u_n(t,r) - \int_0^r K_n(r,\rho)u_n(t,\rho)\,\mathrm{d}\rho, \tag{25}$$

where the kernel $K_n(r,\rho)$ is to be determined, which defined on the domain $\mathcal{T}_k = \{(r,\rho) \in \mathbb{R}^2; 0 \le \rho \le r \le R\}$, to convert the unstable system (17)–(18) into an exponentially stable target system:

$$w_{nt}(t,r) = \frac{\varepsilon}{r}(r w_{nr})_r - \frac{\varepsilon n^2}{r^2}w_n - c w_n, \tag{26}$$

$$w_n(t,R) = 0, \tag{27}$$

where constant $c > 0$ is an adjustable convergence rate. From (18) and (25), let $r = R$, we obtain the boundary control

$$U_n(t,r) = \int_0^R K_n(R,\rho)u_n(t,\rho)\,\mathrm{d}\rho. \tag{28}$$

By substituting the transformation (25) into target system (26)–(27), using two times integrating by parts and taking into account original system (17)–(18), one gets the following equation for kernel K_n

$$\frac{(rK_{nr})_r}{r} - \left(\rho\left(\frac{K_n}{\rho}\right)_\rho\right)_\rho = \left(\frac{n^2}{r^2} - \frac{n^2}{\rho^2} + \frac{\lambda(\rho)+c}{\varepsilon}\right)K_n, \tag{29}$$

$$K_n(r,r) = -\int_0^r \frac{\lambda(\rho)+c}{2\varepsilon}\,\mathrm{d}\rho, \tag{30}$$

$$K_n(r,0) = 0. \tag{31}$$

Theorem 1. *Under the assumption that $\lambda(r)$ is an even analytic function in $[0,R]$, then for a give $n \in \mathbb{Z}$, there is a unique solution $K_n(r,\rho)$ for (29)–(31).*

Due to the radial singularity, the traditional technical route of transforming the kernel PDE into an integral equation and then solving it by using the successive approximation method is inapplicable. Here, the kernel equation is solved directly by the use of a power series, which can be proved to be well-defined and converge (see Theorem 2 in our work Vazquez et al., 2023 for the detailed proof). We employ the theory of power series to give the numerical solution of the kernel function in Section 6.

3.3.1. Transformation between u_n and w_n system

When $K_n(r,\rho)$ is bounded and integrable, the map (25) is reversible and its inverse transformation is

$$u_n(t,r) = w_n(t,r) + \int_0^r L_n(r,\rho)w_n(t,\rho)\,\mathrm{d}\rho. \tag{32}$$

Similar to $K_n(r,\rho)$, L_n is satisfied the following PDE

$$\frac{(rL_{nr})_r}{r} - \left(\rho\left(\frac{L_n}{\rho}\right)_\rho\right)_\rho = \left(\frac{n^2}{r^2} - \frac{n^2}{\rho^2} - \frac{\lambda(\rho)+c}{\varepsilon}\right)L_n, \tag{33}$$

$$L_n(r,r) = \int_0^r \frac{\lambda(\rho)+c}{2\varepsilon}\,\mathrm{d}\rho, \tag{34}$$

$$L_n(r,0) = 0. \tag{35}$$

where $L_n(r,\rho)$ is a bounded and integrable kernel. From Lemma 5, there exist constants $D_1, D_2 > 0$ such that

$$\|w_n(t,\cdot)\|_{L^2}^2 \le D_1\|u_n(t,\cdot)\|_{L^2}^2, \tag{36}$$

$$\|u_n(t,\cdot)\|_{L^2}^2 \le D_2\|w_n(t,\cdot)\|_{L^2}^2. \tag{37}$$

3.3.2. Closed-loop stability analysis of unstable mode

Lemma 2. *For all $n \in \mathbb{Z}$, and for $c \ge c_1$, where $c_1 = D/2 - \varepsilon/(4R^2)$, the equilibrium $w_n \equiv 0$ of system (26)–(27) is exponentially stable, i.e., there exists a positive constant D such that*

$$\|w_n(t,\cdot)\|_{L^2}^2 \le e^{-Dt}\|w_n(0,\cdot)\|_{L^2}^2, \tag{38}$$

where D is independent of n.

Proof. Consider the Lyapunov function:

$$V_2(t) = \frac{1}{2}\|w_n(t,r)\|_{L^2}^2, \tag{39}$$

then, taking its time derivative and using (19), we obtain

$$\dot{V}_2 \le -\left(\frac{\varepsilon_R}{4R^2} + c\right)\|w_n(t,\cdot)\|_{L^2}^2. \tag{40}$$

Choosing $c_1 = D/2 - \varepsilon/(4R^2)$, we then obtain, independent of the value of n, $\dot{V}_2 \le -DV_2$, thus proving the result.

Combining Lemma 2 with the norm equivalence between u_n and w_n system presented by (36) and (37), it is easy to obtain

$$\begin{aligned}&\|u_n(t,\cdot)\|_{L^2}^2 \le D_2\|w_n(t,\cdot)\|_{L^2}^2 \\ \le& D_2 e^{-Dt}\|w_n(0,\cdot)\|_{L^2}^2 \le D_1 D_2 e^{-Dt}\|u_n(0,\cdot)\|_{L^2}^2. \end{aligned} \tag{41}$$

Let $C = D_1 D_2$, we get the following lemma to state the closed-loop exponentially stability.

Lemma 3. *For $|n| \le \bar{N}$, let c_1 be chosen as in Lemma 2. The system (17)–(18) with boundary control (28) is closed-loop exponentially stable, i.e., there exist positive constants C and D such that*

$$\|u_n(t,\cdot)\|_{L^2}^2 \le Ce^{-Dt}\|u_n(0,\cdot)\|_{L^2}^2, \tag{42}$$

where C and D is independent of n, which only depend on the system parameter and the definitional domain.

3.4. The result in physical space

Next, let us return the results of control and stability analysis from Fourier space to physical space. According to (14), reassembling all U_n, we have

$$U(t,\theta) = \sum_{n=-\infty}^{n=\infty} U_n(t,\theta)e^{in\theta}$$

$$= \sum_{n=-\bar{N}}^{\bar{N}} \int_0^r K_n(r,\rho)u_n(t,\rho)\,\mathrm{d}\rho e^{\mathrm{i}n\theta}$$

$$= \int_0^r \int_{-\pi}^{\pi} \sum_{n=-\bar{N}}^{\bar{N}} \frac{K_n(r,\rho)}{2\pi} e^{\mathrm{i}n(\theta-\psi)} u(t,\rho,\psi)\,\mathrm{d}\psi\,\mathrm{d}\rho. \tag{43}$$

From Lemmas 1 and 3, it is clear that only a finite number of modes are unstable, which means only a finite number of K_n, $|n| \le \bar{N}$, are needed, so one can set $U_n = 0$ for $|n| > \bar{N}$, which is applied in the second line of (43). Thus, the integration and (finite) summation can be directly interchanged. Define

$$K(r,\rho,\theta,\psi) = \sum_{n=-\bar{N}}^{n=\bar{N}} \frac{K_n(r,\rho)}{(2\pi)} e^{\mathrm{i}n(\theta-\psi)}. \tag{44}$$

Thus, we arrive the boundary control

$$U(t,\theta) = \mathcal{K}\{u\}(t,\theta), \tag{45}$$

where the operator $\mathcal{K}\{\cdot\}$ is control acting on $u(t,r,\theta)$ in a simple form as

$$\mathcal{K}\{u\}(t,\theta) = \int_0^R \int_{-\pi}^{\pi} K(R,\rho,\theta,\psi)u(t,r,\psi)\,\mathrm{d}\psi\,\mathrm{d}\rho. \tag{46}$$

Combining (5), (6) and (45), the control law for leaders is given by

$$v(t,R,\theta) = \bar{v}(R,\theta) + \mathcal{K}\{v\}(t,\theta) - \mathcal{K}\{\bar{v}\}(t,\theta), \tag{47}$$

$$z(t,R,\theta) = \bar{z}(R,\theta) + \mathcal{K}_z\{z\}(t,\theta) - \mathcal{K}_z\{\bar{z}\}(t,\theta), \tag{48}$$

to achieve the deployment profile $(\bar{v},\bar{z})$.

Theorem 2. *The system (3) with boundary control law (47) and initial condition $v_0(r,\theta) \in L^2$ is exponentially stable in the L^2 norm at the equilibrium $v(t,r,\theta) \equiv \bar{v}(r,\theta)$, i.e., then there exist constants C and $D > 0$ such that*

$$\|v(t,\cdot) - \bar{v}(\cdot)\|_{L^2}^2 \le 2\pi C e^{-Dt}\|v_0 - \bar{v}\|_{L^2}^2. \tag{49}$$

Proof. According to Parseval's Theorem, the L^2 norm of the state in physical space can be obtained by aggregating L^2 norm in all modes. Therefore, applying Lemmas 1 and 3, we get

$$\|u(t,\cdot)\|_{L^2}^2 = 2\pi \sum_{n=-\infty}^{n=\infty} \int_0^R |u_n(t,r)|^2 r\,\mathrm{d}r$$

$$\le 2\pi C e^{-Dt} \sum_{|n|\le\bar{N}} \|u_n(0,\cdot)\|_{L^2}^2 + 2\pi e^{-Dt} \sum_{|n|>\bar{N}} \|u_n(0,\cdot)\|_{L^2}^2$$

$$\le 2\pi C e^{-Dt}\|u(0,\cdot)\|_{L^2}^2, \tag{50}$$

where note that $C > 1$. Due to $u = v - \bar{v}$, we get (49). Thus, the theorem is proved.

Similar results hold for the real-valued system $z(t,r,\theta)$.

4. Observer design

In last section, feedback control (47)–(48) needs the leaders to be aware of the location information of all the agents at all times, which results in overburden communication network traffic load. To address this challenge, we pose the following observer for (11)–(12) to estimate the position of all agents by measuring the state of the leader and its neighbors:

$$\hat{u}_t(t,r,\theta) = \frac{\varepsilon(r\hat{u}_r)_r}{r} + \frac{\varepsilon\hat{u}_{\theta\theta}}{r^2} + \lambda(r)\hat{u} + T(t,R,r,\theta), \tag{51}$$

$$\hat{u}(t,R,\theta) = U(t,\theta) + q_0(u_r(t,R,\theta) - \hat{u}_r(t,R,\theta)), \tag{52}$$

which has the same structure as the system in addition to the output feedback item. Here, the output injection operator T is given by

$$T(t,R,r,\theta) = \int_{-\pi}^{\pi} \frac{q_1(R,r,\theta-\psi)}{2\pi}(u_r(t,R,\psi) - \hat{u}_r(t,R,\psi))\,\mathrm{d}\psi, \tag{53}$$

where q_1 and q_0 are the observer gains need to be found to guarantee exponential convergence of the error dynamics between $\hat{u}$ and u. $\hat{u}$ is the estimated state, and U is the applied control. By introducing the error variable $\tilde{u} = u - \hat{u}$, we obtain the error system as following

$$\tilde{u}_t(t,r,\theta) = \frac{\varepsilon(r\tilde{u}_r)_r}{r} + \frac{\varepsilon\tilde{u}_{\theta\theta}}{r^2} + \lambda(r)\tilde{u} - \int_{-\pi}^{\pi} \frac{q_1(R,r,\theta-\psi)}{2\pi}\tilde{u}_r(t,R,\psi)\,\mathrm{d}\psi, \tag{54}$$

$$\tilde{u}(t,R,\theta) = -q_0\tilde{u}_r(t,R,\theta). \tag{55}$$

Next, we utilize a similar method as Section 3 to design the kernel function. First, using a Fourier series to expand the system (54) and the boundary condition (55),

$$\tilde{u}(t,r,\theta) = \sum_{n=-\infty}^{n=\infty} \tilde{u}_n(t,r)e^{\mathrm{i}n\theta}, \tag{56}$$

$$T(t,R,r,\theta) = \sum_{n=-\infty}^{n=\infty} T_n(R,r)e^{\mathrm{i}n\theta}, \tag{57}$$

where the coefficients are defined as

$$\tilde{u}_n(t,r) = \frac{1}{2\pi}\int_{-\pi}^{\pi} \tilde{u}(t,r,\psi)e^{-\mathrm{i}n\psi}\,\mathrm{d}\psi, \tag{58}$$

$$T_n(t,R,r) = q_{1n}(R,r)\tilde{u}_{nr}(t,R). \tag{59}$$

Thus, we gets $\tilde{u}_n$ system that does not depend on θ, as follows

$$\tilde{u}_{nt}(t,r) = \frac{\varepsilon}{r}(r\tilde{u}_{nr})_r - \frac{\varepsilon n^2}{r^2}\tilde{u}_n + \lambda(r)\tilde{u}_n - T_n(R,r), \tag{60}$$

$$\tilde{u}_n(t,R) = -q_0\tilde{u}_{nr}(t,R). \tag{61}$$

4.1. Open-loop stability properties in Fourier space

Similar to control, the large modes themselves are exponential stable and converge at the expected decay rate. First, we analyze the stability of the observer without output feedback item T_n, as follow

$$\hat{u}_{nt}(t,r) = \frac{\varepsilon}{r}(r\hat{u}_{nr})_r - \frac{\varepsilon n^2}{r^2}\hat{u}_n + \lambda(r)\hat{u}_n, \tag{62}$$

$$\hat{u}_n(t,R) = 0, \tag{63}$$

$$\tilde{u}_{nt}(t,r) = \frac{\varepsilon}{r}(r\tilde{u}_{nr})_r - \frac{\varepsilon n^2}{r^2}\tilde{u}_n + \lambda(r)\tilde{u}_n, \tag{64}$$

$$\tilde{u}_n(t,R) = 0. \tag{65}$$

Lemma 4. *There exists $\bar{N} \in \mathbb{N}$ such that, for all $|n| > N$, the equilibrium $\hat{u}_n \equiv \tilde{u}_n \equiv 0$ of system (62)–(65) is open loop exponentially stable, i.e., for $\hat{u}_n(t,R) = 0$ and $\tilde{u}_n(t,R) = 0$, there exists a positive constant D, such that*

$$\|\hat{u}_n(t,\cdot)\|_{L^2}^2 + \|\tilde{u}_n(t,\cdot)\|_{L^2}^2 \le e^{-Dt}\left(\|\hat{u}_n(0,\cdot)\|_{L^2}^2 + \|\tilde{u}_n(0,\cdot)\|_{L^2}^2\right), \tag{66}$$

where D is independent of n.

4.2. Observation for unstable modes

Now the backstepping method is utilized to find the observer gain for the modes $|n| < \bar{N}$. Using the transformation

$$\tilde{u}_n(t,r) = \tilde{w}_n(t,r) - \int_r^R Q_n(r,\rho)\tilde{w}_n(t,\rho)\,\mathrm{d}\rho, \tag{67}$$

where Q_n is kernel function to be determined, which defined on the domain $\mathcal{T}_q = \{(r,\rho) \in \mathbb{R}^2; 0 \le r \le \rho \le R\}$, convert the error system (60)–(61) to a exponentially stable target system as follows:

$$\tilde{w}_{nt}(t,r) = \frac{\varepsilon}{r}(r\tilde{w}_{nr})_r - \frac{\varepsilon n^2}{r^2}\tilde{w}_n - c\tilde{w}_n, \tag{68}$$

$$\tilde{w}_n(t,R) = 0. \tag{69}$$

By substituting the transformation (67) into error system (60)–(61), using two times integrating by parts and taking into account target system (68)–(69), then observer kernel Q_n satisfies the following PDE

$$\frac{(rQ_{nr})_r}{r} - \left(\rho\left(\frac{Q_n}{\rho}\right)_\rho\right)_\rho = \left(\frac{n^2}{r^2} - \frac{n^2}{\rho^2} - \frac{\lambda(\rho)+c}{\varepsilon}\right)Q_n, \tag{70}$$

with boundary condition

$$Q_n(r,r) = Q_n(R,R) + \int_r^R \frac{\lambda(\rho)+c}{2\varepsilon}\,\mathrm{d}\rho. \tag{71}$$

Simultaneously, the boundary conditions determine the observer gains as

$$q_{1n}(r,R) = \varepsilon Q_n(r,R), \qquad q_0 = 0. \tag{72}$$

The stability of the observer can be established similarly as the controller, so we omit it to save space.

4.3. The result in physical space

Return the results of the observer and stability analysis from Fourier space to physical space. Taking advantage of Fourier series on transformation (67) and the coefficient, reassembling all Q_n and substituting T into (51), we get the observer

$$\hat{u}_t = \frac{\varepsilon}{r}(r\hat{u}_r)_r + \frac{\varepsilon}{r^2}\hat{u}_{\theta\theta} + \lambda(r)\hat{u} + T(t,R,r,\theta), \tag{73}$$

$$\hat{u}(t,R,\theta) = U(t,\theta), \tag{74}$$

where

$$T(t,R,r,\theta) \tag{75}$$

$$= \int_{-\pi}^{\pi}\sum_{n=-\bar{N}}^{\bar{N}} \frac{Q_n(r,R)}{2\pi}e^{\mathrm{i}n(\theta-\psi)}(u_r(t,R,\psi) - \hat{u}_r(t,R,\psi))\,\mathrm{d}\psi.$$

Define an observer operator $\mathcal{Q}\{\cdot\}$ acting on $v_r(t,R,\theta)$ as follows

$$\mathcal{Q}\{v_r\} = \int_{-\pi}^{\pi}\sum_{n=-\bar{N}}^{\bar{N}} \frac{Q_n(r,R)}{2\pi}e^{\mathrm{i}n(\theta-\psi)}v_r(t,R,\psi)\,\mathrm{d}\psi. \tag{76}$$

Combining (5), (6) (45) and (73), the observer-based feedback control is given by

$$\hat{v}_t = \frac{\varepsilon}{r}(r\hat{v}_r)_r + \frac{\varepsilon}{r^2}\hat{v}_{\theta\theta} + \lambda(r)\hat{v} + \mathcal{Q}\{v_r\} - \mathcal{Q}\{\hat{v}_r\}, \tag{77}$$

$$\hat{v}(t,R,\theta) = \bar{v}(R,\theta) + \mathcal{K}\{\hat{v}\}(t,\theta) - \mathcal{K}\{\bar{v}\}(t,\theta). \tag{78}$$

According to Parseval's Theorem, the L^2 norm of the state in physical space can be obtained by aggregating L^2 norm in all modes. According to the separation principle, we get the final result.

Theorem 3. *The system (3), (5) with boundary control law (47), the observer (77)–(78) and initial condition $v_0(r,\theta)$, $\hat{v}_0(r,\theta) \in L^2$ are exponentially stable in the L^2 norm, i.e., there exist constants C_0 and $D > 0$ such that*

$$\begin{aligned}&\|v-\bar{v}\|_{L^2}^2 + \|\hat{v}-\bar{v}\|_{L^2}^2\\ \le& 2\pi C_0 e^{-Dt}(\|v_0-\bar{v}\|_{L^2}^2 + \|\hat{v}_0-\bar{v}\|_{L^2}^2).\end{aligned}$$

Similar results hold for the real-valued system $z(t,r,\theta)$.

5. Discretized control protocol

The PDE model (3)–(4) with control (47)–(48) and observer (77)–(78) is discretized in the space to obtain a discrete protocol for a finite number of agent, namely the coefficients in (1) and the control in (2). In the discretization process, the continuous states $v(t,r,\theta)$ are rewritten as discrete positional states $v(t,r_i,\theta_j)$ that denotes the position of agent (i,j) at time t. To avoid the singular in the disk center, the grid defined in Lai (2001) is employed, as follows:

$$r_i = \left(i - \frac{1}{2}\right)h_r, \quad \theta_j = (j-1)h_\theta, \tag{79}$$

where $h_r = R/(M-\frac{1}{2})$, $h_\theta = 2\pi/N$, and $i = 1,\dots,M$, $j = 1,\dots,N$.

Before showing the control protocol, the following proposition is given to discuss the error between the discrete model and reaction–diffusion PDE-based dynamics.

Theorem 4. *Consider a MAS with $M \times N$ agents on mesh-grid disk topology. Defined the spatial steps $h_r = R/(M-\frac{1}{2})$, $h_\theta = 2\pi/N$, and location $r_i = \left(i-\frac{1}{2}\right)h_r$, $\theta_j = (j-1)h_\theta$. The discrete ODE model (1) and the continuum diffusion–reaction PDE (3)–(4) are equivalent in the sense that the discrete solution approaches the continuous solution, with approximating error $O(h_r^2 + h_\theta^2)$.*

Proof. Expanding each of the function values of v in a Taylor series about the point (r_i,θ_j), we have (LeVeque, 2007)

$$\begin{aligned}v(r_{i\pm1},\theta_j) =\ & v(r_i,\theta_j) \pm \partial_r v(r_i,\theta_j)h_r + \partial_{rr}v(r_i,\theta_j)\frac{h_r^2}{2!}\\ & \pm\partial_{rrr}v(r_i,\theta_j)\frac{h_r^3}{3!} + \mathcal{O}(h_r^4),\end{aligned} \tag{80}$$

where ∂_r denotes the partial derivative with respect to r. One obtains similar expanded forms for $v(r_i,\theta_{j\pm1})$. Using (80) allows us to obtain that

$$\begin{aligned}&\frac{v(r_{i+1},\theta_j) - 2v(r_i,\theta_j) + v(r_{i-1},\theta_j)}{h_r^2}\\ =\ & \frac{1}{h_r^2}\Big(2v(r_i,\theta_j) + 2\partial_{rr}v(r_i,\theta_j)\frac{h_r^2}{2!}\\ & \qquad -2v(r_i,\theta_j) + \mathcal{O}(h_r^4)\Big)\\ =\ & \partial_{rr}v(r_i,\theta_j) + \mathcal{O}(h_r^2),\end{aligned} \tag{81}$$

Similarly, we give that

$$\frac{v(r_{i+1},\theta_j) - v(r_{i-1},\theta_j)}{2h_r} = \partial_r v(r_i,\theta_j) + \mathcal{O}(h_r^2), \tag{82}$$

$$\begin{aligned}&\frac{v(r_i,\theta_{j+1}) - 2v(r_i,\theta_j) + v(r_i,\theta_{j-1})}{h_\theta^2}\\ =\ & \partial_{\theta\theta}v(r_i,\theta_j) + \mathcal{O}(h_\theta^2).\end{aligned} \tag{83}$$

The calculations above establish the link between the discrete model and the continuous PDE, and confirm that the approximation is second-order accurate. The approximating error due

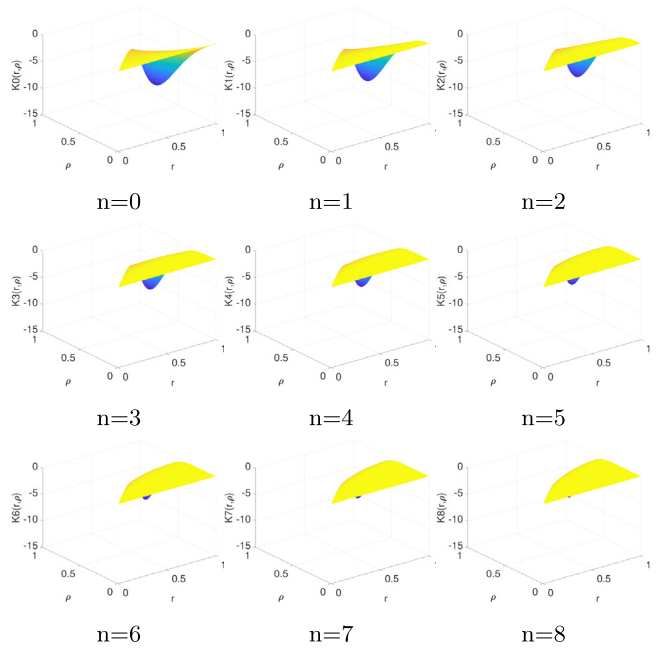

Fig. 3. Polynomial approximations of kernel for different modes.

to the discretization is $O(h_r^2 + h_\theta^2)$ which depends on the spatial finite difference method. As the number of agents increases, the approximating error decreases, thus the PDE-based method is suitable for large systems.

In the sequel, $v(r_i, \theta_j)$ is abbreviated as $v_{i,j}$ for save space.

5.1. Followers' control protocol

Using three-point central difference method to approximate the spatial derivatives in (3), we obtain the followers' control protocols:

For $i = 2, 3, \ldots, M-1, j = 1, 2, 3, \ldots, N$,

$$\begin{aligned}\dot{v}_{i,j}(t) =& \varepsilon \frac{\left(v_{i+1,j} - v_{i,j}\right) - \left(v_{i,j} - v_{i-1,j}\right)}{h_r^2} \\ &+ \frac{\varepsilon}{r_i}\frac{v_{i+1,j} - v_{i-1,j}}{2h_r} + \frac{\varepsilon}{r_i^2}\frac{v_{i,j+1} - 2v_{i,j} + v_{i,j-1}}{h_\theta^2} \\ &+ \lambda_i v_{i,j}. \end{aligned} \tag{84}$$

For $i = 1, j = 1, 2, \ldots, N$, thanks to the half-grid, $v_{0,j}$ are eliminated, so

$$\begin{aligned}\dot{v}_{1,j}(t) =& \varepsilon \frac{v_{2,j} - 2v_{1,j}}{h_r^2} + \frac{\varepsilon}{r_1}\frac{v_{2,j}}{2h_r} \\ &+ \frac{\varepsilon}{r_1^2}\frac{v_{1,j+1} - 2v_{1,j} + v_{1,j-1}}{h_\theta^2} + \lambda_1 v_{1,j}. \end{aligned} \tag{85}$$

Here we should note that θ is periodic of 2π, therefore $v_{i,-1} = v_{i,N}$ and $v_{i,N+1} = v_{i,0}$. Similar protocols can be given for z-axis.

5.2. Leaders' control protocol

Next, the leaders' control protocol will be given. We use the Simpson's 1/3 rule to approximate the integral in (47), and define a operator $\bar{\mathcal{K}}\{.\}$, acting on the agents' position vector $[v_{11}(t), v_{21} \ldots, v_{M1}, \ldots, v_{ij}, \ldots, v_{MN}]^T$, which is the corresponding discrete form of (46), thus obtain

$$\bar{\mathcal{K}}\{v\}(\theta) = \sum_{i=1}^{M}\sum_{l=1}^{N} a_{i,l} K_{i,l}^j v_{i,l}(t), \tag{86}$$

where $K_{i,l}^j = K(R, r_i, \theta_j, \psi_l)$. The numerical solution method of $K_{i,l}^j$ will be given later. Given Simpson's rule, M and N should be chosen as odd number, as even. The coefficients $a_{i,l}$ are determined by Simpson integral rules.

Thus, the leaders' control protocols are

$$v_{M,j} = \bar{v}_{M,j} + \bar{\mathcal{K}}\{v\} - \bar{\mathcal{K}}\{\bar{v}\}, \tag{87}$$

Through the above discrete control protocol, it is easy to notice that the followers only need the states of their neighbors on the communication topology, and the information that leaders need includes the real-time status and desired deployment of all the agents. Discretizing the state observer in a similar manner yields a discretized observer form as follows,

$$\begin{aligned}\dot{\hat{v}}_{i,j} =& \varepsilon \frac{\left(\hat{v}_{i+1,j} - \hat{v}_{i,j}\right) - \left(\hat{v}_{i,j} - \hat{v}_{i-1,j}\right)}{h_r^2} + \lambda_i \hat{v}_{i,j} \\ &+ \frac{\varepsilon}{r_i}\frac{\hat{v}_{i+1,j} - \hat{v}_{i-1,j}}{2h_r} + \frac{\varepsilon}{r_i^2}\frac{\hat{v}_{i,j+1} - 2\hat{v}_{i,j} + \hat{v}_{i,j-1}}{h_\theta^2} \\ &+ \sum_{l=0}^{N}\sum_{n=-\bar{N}}^{\bar{N}} b_l \frac{Q_{n,i}}{2\pi} e^{in((j-1)-(l-1))h_\theta} \cdot \\ &\left(\frac{v_{M,l} - v_{M-1,l}}{h_r} - \frac{\hat{v}_{M,l} - \hat{v}_{M-1,l}}{h_r}\right), \end{aligned} \tag{88}$$

where $Q_{n,i} = Q_n(r_i, R)$ and b_l is the coefficient of Simpson's rule. The spatial derivatives of all leaders are transmitted to the observer to estimate the position of all agents. Integrate it into the boundary control mentioned above, the real-time positions of the leaders' protocol (87) are replaced by their estimated states, then we obtain the leaders' protocol with the output feedback control, as follows

$$v_{M,j} = \bar{v}_{M,j} + \bar{\mathcal{K}}\{\hat{v}\} - \bar{\mathcal{K}}\{\bar{v}\}, \tag{89}$$

Here, the observer provides estimated values $\hat{v}_{i,j}$ by measuring $v_r(t, R, \theta)$ to replace the real-states of followers $v_{i,j}$. In particular, the measurement is discretized as

$$v_r(R, \theta) = \frac{v_{M,j} - v_{M-1,j}}{h_r}, \tag{90}$$

which avoids the issue that the spatial derivative is difficult to be accurately measured.

Remark 2. Appropriately increasing the complexity of the communication topology, when the leader can obtain the second-closest information, the spatial derivative of the leader with respect to r is given by

$$v_r(R, \theta) = \frac{3v_{M,j} - 4v_{M-1,j} + v_{M-2,j}}{2h_r}, \tag{91}$$

This approximation is second order accurate. Compared to the resources required to obtain all agent positions, the observer needs fewer communication resources.

Hereto, a multi-agent 3-D deployment model that only requires local information interaction is given.

5.3. Numerical approximation of the kernels

The main idea of this section is to approximate kernel functions by using the power series to find numerical solution of the kernels. The solution techniques for the spatial-varying kernel equations are available (Camacho-Solorio et al., 2020). For the kernel functions of control (29)–(31), let us make the change $K_n(r, \rho) = G_n(r, \rho)\rho\left(\frac{\rho}{r}\right)^{|n|}$ to facilitate the subsequent calculations, gets

$$G_{nrr} + \frac{1 - 2|n|}{r}G_{nr} - G_{n\rho\rho} - \frac{1 + 2|n|}{\rho}G_{n\rho}$$

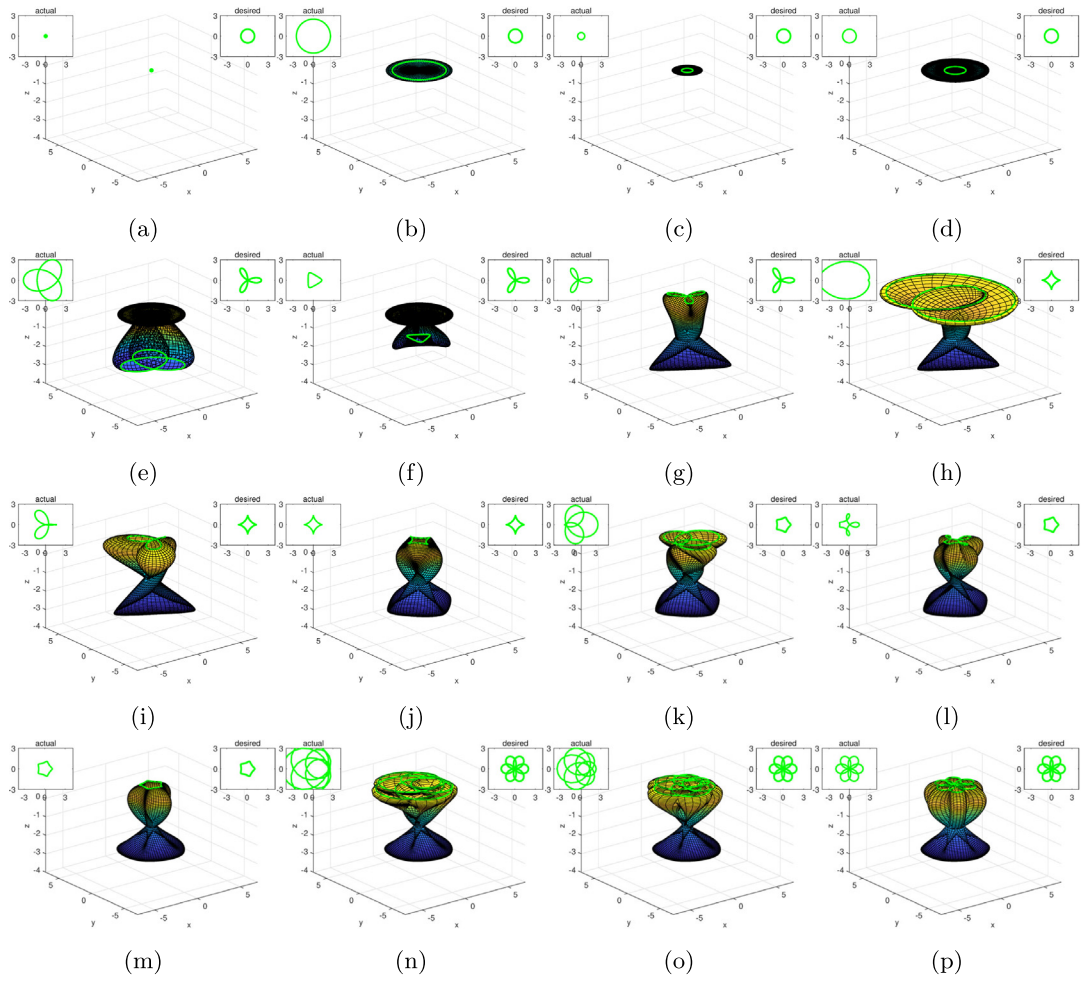

Fig. 4. Agents deployment snapshots. (For interpretation of the references to color in this figure legend, the reader is referred to the web version of this article.)

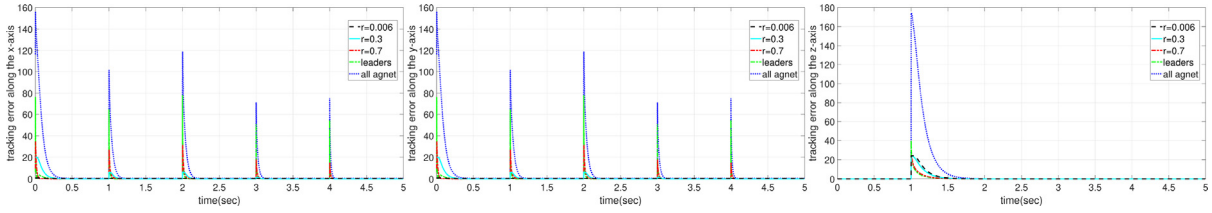

Fig. 5. The tracking errors of the agents on the x, y, and z-axis, respectively, when the observer is not implemented.

$$= \frac{\lambda(\rho)+c}{\varepsilon} G_n, \tag{92}$$

$$G_n(r,r) = -\frac{1}{r}\int_0^r \frac{\lambda(\rho)+c}{2\varepsilon}\,\mathrm{d}\rho. \tag{93}$$

The numerical approximation of the kernels are obtained by the mth power series as following

$$G_n^m(r,\rho) = \sum_{i=0}^{m}\sum_{j=0}^{m-i} b_{ij} r^i \rho^j, \tag{94}$$

where $b_{ij} \in \mathbb{R}$ are to be calculated from (92)–(93). Similarly, the term $\lambda(\rho)+c$ can be approximated as (c is compressed for notational brevity)

$$\lambda(\rho)+c = \sum_{l=0}^{L} \lambda_l \rho^l, \tag{95}$$

where $\lambda_l \in \mathbb{R}$ are L-order power series coefficients of $\lambda(\rho)+c$. As thus, the problem of solving kernels becomes how to find the coefficients b_{ij}. The total number of b_{ij} is $N_b = (m+2)(m+1)/2$.

As the derivative term and the fractional term on the left-hand side of (92), a m-order power series approximation is substituted into it, that is

$$\begin{aligned}
&\frac{\partial^2 G_n^m}{\partial r^2} + \frac{(1-2|n|)}{r}\frac{\partial G_n^m}{\partial r} - \frac{\partial^2 G_n^m}{\partial \rho^2} - \frac{(1+2|n|)}{\rho}\frac{\partial G_n^m}{\partial \rho} \\
&= (1-2|n|)\sum_{j=0}^{m-1} b_{1j} r^{-1}\rho^j - (1+2|n|)\sum_{i=0}^{m-1} b_{i1} r^i \rho^{-1} \\
&\quad + \sum_{i=0}^{m-2}\sum_{j=0}^{m-i-2}\big((i+2)(i+2-2|n|)b_{i+2,j}\big) r^i \rho^j \\
&\quad - \sum_{i=0}^{m-2}\sum_{j=0}^{m-i-2}\big((j+2)(j+2+2|n|)b_{i,j+2}\big) r^i \rho^j.
\end{aligned} \tag{96}$$

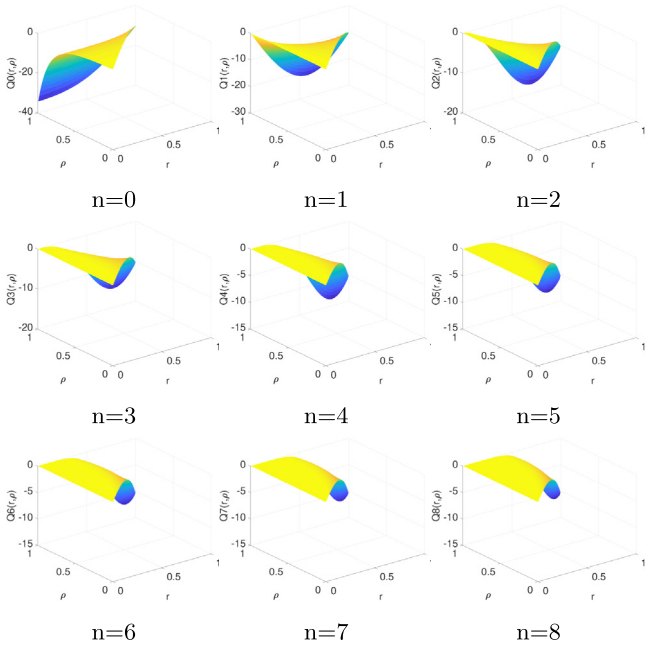

Fig. 6. Polynomial approximations of observer kernel for different modes.

The right-hand side is:

$$\frac{\lambda(\rho)+c}{\varepsilon}G_n = \left(\sum_{l=0}^{L}\frac{\lambda_l}{\varepsilon}\rho^l\right)\left(\sum_{i=0}^{m}\sum_{j=0}^{m-i}b_{ij}r^i\rho^j\right) = \sum_{l=0}^{L}\sum_{i=0}^{m}\sum_{j=l}^{m-i+l}\frac{\lambda_l b_{i,j-l}}{\varepsilon}r^i\rho^j, \tag{97}$$

Note that in order to correspond to the left-hand side, the first $m-2$ order items are taken, then

$$\frac{\lambda(\rho)+c}{\varepsilon}G_n = \sum_{l=0}^{m-2}\sum_{i=0}^{m-2}\sum_{j=l}^{m-i-2}\frac{\lambda_l b_{i,j-l}}{\varepsilon}r^i\rho^j, \tag{98}$$

Thus, all power $r^i\rho^j$ satisfy the following equations:
(1) for $0\le i\le m-2, 0\le j\le m-2-i$,

$$(i+2)(i+2-2|n|)b_{i+2,j} - (j+2)(j+2+2|n|)b_{i,j+2} - \sum_{l=0}^{m-2}\frac{\lambda_l b_{i,j-l}}{\varepsilon} = 0,$$

(2) for $0\le i\le m-1$, $b_{i1}=0$,
(3) for $0\le j\le m-1$, $7b_{1j}=0$.

In the same manner, (93) is rewritten as

$$G_n^m(r,r)+\frac{1}{r}\int_{R_1}^{r}\frac{\lambda(\rho)+c}{2\varepsilon}d\rho = \sum_{i=0}^{m}\sum_{j=0}^{m-i}b_{ij}r^{i+j}+\sum_{l=0}^{L}\frac{\lambda_l}{2\varepsilon(l+1)}r^l, \tag{99}$$

which brings

$$\begin{cases} b_{ij} = -\dfrac{\lambda_l}{2\varepsilon(l+1)}, & i+j=l,\\ b_{ij}=0, & i+j\neq l. \end{cases} \tag{100}$$

Thus, we obtain a system of equations for b_{ij}, which is easy to solve.

Table 1
Desired shape of leaders and coefficients of Fig. 4.

Desired shape of leaders		Coefficients	
		$f(\theta)$	g
(i)	•	0	0
(ii)	○	$e^{i\theta}$	0
(iii)	✂	$e^{i\theta}+e^{-2i\theta}$	1
(iv)	✧	$e^{i\theta}+(1/3)e^{-3i\theta}$	1
(v)	⬠	$e^{i\theta}+(1/8)e^{-4i\theta}$	1
(vi)	❀	$e^{i\theta}+e^{-5i\theta}$	1

6. Simulation

We consider a case with 81×87 agents on 3-D space, in which the leader agents are controlled by (87), and the followers are governed by (84) with the decay rate $c=4$. The system parameters are set as $R=1$, $\varepsilon=1$, $\varepsilon_z=1$, $\lambda=40-20\cos(\pi r)$, $\mu=50r^2$. Before deploying the formation, we need to calculate a finite number of numerical solutions of K_n, which shown in Fig. 3. As $K_{-n}=K_n$, here only show K_n, $n=0,1,\ldots,8$.

Our first simulation experiment focused on the transition between six different desired deployment profiles, and a series of snapshots in Fig. 4 display this dynamical deployment process. The parameter of desired profiles are summarized in Table 1. Initially, all the agents are at the origin (0, 0, 0), shown as Fig. 4(a). Fig. 4(d), (g), (j), (m), (p) are desired profiles, and the rest of figures are transients. The solid green line indicates the leaders. The insets (on the upper-left corner) show the actual formation of the leaders, that is the control $(v(R,\theta), z(R,\theta))$ in (47)–(48), and the desired boundary formation is illustrated by the insets on upper right corner. A video of the simulation can be downloaded from Zhang et al. (2019).

The time evolution of L^2 norm of the tracking error $\|(v-\bar{v})\|_{L^2}^2$ for the selected layers $r=0.006$, $r=0.3$, $r=0.7$, the leader layer $r=1$ and all agents along the x-axis, y-axis, z-axis respectively are shown in Fig. 5. As you can see, the tracking errors suddenly increase when a new desired deployment is given, and then rapidly converge to zero.

The second simulation experiment demonstrates the effectiveness of the output feedback control, using the same parameters as the previous one. Fig. 6 depicts the approximate numerical solution of the observer kernels Q_n. The observer's initial condition is set as the agents' actual position plus a Gaussian distributed error with zero mean and $\delta=0.1$. Fig. 7(a) shows the L^2 norm of tracking error, while, the observer is plotted in 7(b). Obviously, after implementing the observer, the error is larger than the previous experiment directly using the actual state. However, as the observer's error converges, the tracking errors also converge quickly.

7. Conclusion

In this paper, we have addressed the problem of deployment in 3-D space by two diffusion–reaction equations with a non-constant coefficient, from the viewpoint of PDEs as the continuous approximation of a lot of discrete interacting agents. Employing backstepping boundary control, we design a boundary controller for leaders to actuate all agents to desired profile governed by the nonzero equilibrium of the PDEs model. In the same manner, an observer is provided, allowing an output feedback control protocol requiring as sole measurement the leaders' neighbor positions. The merit of our framework is that the agents transform smoothly between different deployments by

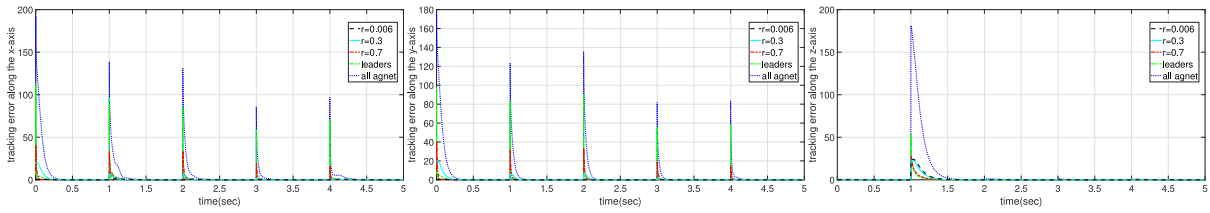

(a) the tracking error

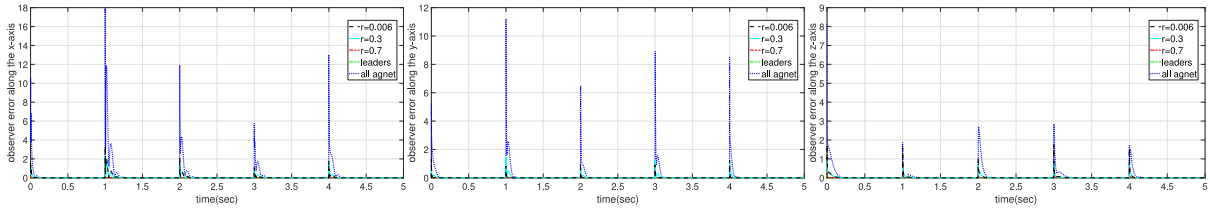

(b) the observer error

Fig. 7. The tracking and observer errors of the agents on the x, y, and z-axis, respectively, when the observer is implemented.

modifying the bias terms in the leader's control protocol, instead of commanding directly the reference trajectory.

Future research includes the extension of this paradigm to the 2-D wave equation model; the methodology of this paper would be applied to obtain an acceleration-level control law. Another possible extension is to consider the impacts of disturbances or delays to make the model more realistic. Moreover, we will investigate the issue of practical implement of multi-robots that is not considered in this study. We consider implementing two layers control framework at the agent level to fix the agent's position by controlling velocity or (more realistically) acceleration.

Appendix

Lemma 5. *Suppose that the functions $g_n(r)$ and $f_n(r)$ are given to each other by the following integral transformations*

$$g_n(r) = f_n(r) - \int_0^r G_n(r,\rho)\rho\left(\frac{\rho}{r}\right)^{|n|} f_n(t,\rho)\,\mathrm{d}\rho, \tag{A.1}$$

$$f_n(r) = g_n(r) + \int_0^r G_n^*(r,\rho)\rho\left(\frac{\rho}{r}\right)^{|n|} g_n(\rho)\,\mathrm{d}\rho, \tag{A.2}$$

where $G_n, G_n^* \in \mathcal{C}^2(\mathcal{T})$, $\mathcal{T} = \{(r,\rho) : 0 \le \rho \le r \le R\}$ and G_n, G_n^* are bounded by $\bar{G}, \bar{G}^*$. Then g_n and f_n are equivalent in L_1 norms, i.e.,

$$\|g_n\|_{L^2}^2 \le C_1\|f_n\|_{L^2}^2, \quad \|f_n\|_{L^2}^2 \le C_2\|g_n\|_{L^2}^2, \tag{A.3}$$

the constants C_1, C_2 only depend on G, G^* and R.

Similarly, suppose that the functions $g_n(t,r)$ and $f_n(t,r)$ are given to each other by the following observer transformations

$$g_n(r) = f_n(r) - \int_r^R P_n(r,\rho)\rho\left(\frac{\rho}{r}\right)^{-|n|} f_n(\rho)\,\mathrm{d}\rho, \tag{A.4}$$

$$f_n(r) = g_n(r) + \int_r^R P_n^*(r,\rho)\rho\left(\frac{\rho}{r}\right)^{-|n|} g_n(\rho)\,\mathrm{d}\rho, \tag{A.5}$$

where $P_n, P_n^* \in \mathcal{C}^2(\mathcal{T}')$, $\mathcal{T}' = \{(r,\rho) : 0 \le r \le \rho \le R\}$ and P_n, P_n^* are bounded by $\bar{P}, \bar{P}^*$. Then,

$$\|g_n\|_{L^2}^2 \le C_3\|f_n\|_{L^2}^2, \quad \|f_n\|_{L^2}^2 \le C_4\|g_n\|_{L^2}^2, \tag{A.6}$$

the constants C_3, C_4 only depend on P, P^* and R.

Proof. Integrating (A.1) and using Cauchy–Schwarz inequality, we have

$$\begin{aligned}\|g_n\|_{L^2}^2 &= \int_0^R \left| f_n - \int_0^r G_n(r,\rho)\rho\left(\frac{\rho}{r}\right)^{|n|} f_n(t,\rho)\,\mathrm{d}\rho\right|^2 r\,\mathrm{d}r\\ &\le 2\|f_n\|_{L^2}^2 + 2\int_0^R \left|\int_0^r G_n(r,\rho)\rho\left(\frac{\rho}{r}\right)^{|n|} f_n(t,\rho)\,\mathrm{d}\rho\right|^2 r\,\mathrm{d}r\\ &\le 2\|f_n\|_{L^2}^2 + 2R^2\bar{G}^2\int_0^R \rho d\rho\int_0^R f_n^2(t,\rho)\rho\,\mathrm{d}\rho,\end{aligned} \tag{A.7}$$

where note that $0 \le \rho \le r \le R$, thus

$$\|g_n\|_{L^2}^2 \le (2 + R^4\bar{G}^2)\|f_n\|_{L^2}^2 = C_1\|f_n\|_{L^2}^2. \tag{A.8}$$

Similarly, from (A.2), (A.4) and (A.5), respectively, we obtain $C_2 = 2 + R^4\bar{G}^{*2}$, $C_3 = 2 + R^4\bar{P}^2$ and $C_4 = 2 + R^4\bar{P}^{*2}$.

References

Auriol, J. (2020). Output feedback stabilization of an underactuated cascade network of interconnected linear PDE systems using a backstepping approach. *Automatica*, *117*, Article 108964.

Bandyopadhyay, S., Chung, S.-J., & Hadaegh, F. Y. (2017). Probabilistic and distributed control of a large-scale swarm of autonomous agents. *IEEE Transactions on Robotics*, *33*(5), 1103–1123.

Camacho-Solorio, L., Vazquez, R., & Krstic, M. (2020). Boundary observers for coupled diffusion–reaction systems with prescribed convergence rate. *Systems & Control Letters*, *135*, Article 104586.

Chen, C. P., Wen, G.-X., Liu, Y.-J., & Liu, Z. (2015). Observer-based adaptive backstepping consensus tracking control for high-order nonlinear semi-strict-feedback multiagent systems. *IEEE Transactions on Cybernetics*, *46*(7), 1591–1601.

Chung, S.-J., Paranjape, A. A., Dames, P., Shen, S., & Kumar, V. (2018). A survey on aerial swarm robotics. *IEEE Transactions on Robotics*, *34*(4), 837–855.

Deutscher, J., & Kerschbaum, S. (2018). Backstepping control of coupled linear parabolic PIDEs with spatially varying coefficients. *IEEE Transactions on Automatic Control*, *63*(12), 4218–4233.

Ferrari-Trecate, G., Buffa, A., & Gati, M. (2006). Analysis of coordination in multi-agent systems through partial difference equations. *IEEE Transactions on Automatic Control*, *51*(6), 1058–1063.

Freudenthaler, G., & Meurer, T. (2020). PDE-based multi-agent formation control using flatness and backstepping: Analysis, design and robot experiments. *Automatica*, [ISSN: 0005-1098] *115*, Article 108897.

Frihauf, P., & Krstic, M. (2010). Leader-enabled deployment onto planar curves: A PDE-based approach. *IEEE Transactions on Automatic Control*, *56*(8), 1791–1806.

Fu, Q., Yu, P., Xu, G., & Wu, J. (2019). Containment control for partial differential multi-agent systems. *Physica A. Statistical Mechanics and its Applications*, Article 121549.

Gazi, V. (2005). Swarm aggregations using artificial potentials and sliding-mode control. *IEEE Transactions on Robotics*, *21*(6), 1208–1214.

Hao, H., & Barooah, P. (2012). Approximation error in PDE-based modelling of vehicular platoons. *International Journal of Control*, *85*(8), 1121–1129.

Hua, C.-C., You, X., & Guan, X.-P. (2016). Leader-following consensus for a class of high-order nonlinear multi-agent systems. *Automatica*, *73*, 138–144.
Koga, S., Krstic, M., & Beaman, J. (2020). Laser sintering control for metal additive manufacturing by PDE backstepping. *IEEE Transactions on Control Systems Technology*, *28*(5), 1928–1939.
Krishnan, V., & Martínez, S. (2018). Distributed control for spatial self-organization of multi-agent swarms. *SIAM Journal on Control and Optimization*, *56*(5), 3642–3667.
Krstic, M., & Smyshlyaev, A. (2008). *Boundary control of PDES: A course on backstepping designs*. SIAM.
Lai, M.-C. (2001). A note on finite difference discretizations for Poisson equation on a disk. *Numerical Methods for Partial Differential Equations: An International Journal*, *17*(3), 199–203.
LeVeque, R. J. (2007). *Finite difference methods for ordinary and partial differential equations: steady-state and time-dependent problems, Vol. 98*. SIAM.
Li, G., & Xie, C. (2010). Feedback stabilization of reaction-diffusion equation in a two-dimensional region. In *49th IEEE conference on decision and control (CDC)* (pp. 2985–2989). IEEE.
Meurer, T., & Krstic, M. (2011). Finite-time multi-agent deployment: A nonlinear PDE motion planning approach. *Automatica*, *47*(11), 2534–2542.
Oh, K.-K., Park, M.-C., & Ahn, H.-S. (2015). A survey of multi-agent formation control. *Automatica*, *53*, 424–440.
Pilloni, A., Pisano, A., Orlov, Y., & Usai, E. (2015). Consensus-based control for a network of diffusion PDEs with boundary local interaction. *IEEE Transactions on Automatic Control*, *61*(9), 2708–2713.
Qi, J., Tang, S.-X., & Wang, C. (2019). Parabolic PDE-based multi-agent formation control on a cylindrical surface. *International Journal of Control*, *92*(1), 77–99.
Qi, J., Vazquez, R., & Krstic, M. (2015). Multi-agent deployment in 3-D via PDE control. *IEEE Transactions on Automatic Control*, *60*(4), 891–906.
Qi, J., Wang, S., Fang, J.-a., & Diagne, M. (2019). Control of multi-agent systems with input delay via PDE-based method. *Automatica*, *106*, 91–100.
Qi, J., Zhang, J., & Ding, Y. (2017). Wave equation-based time-varying formation control of multiagent systems. *IEEE Transactions on Control Systems Technology*, *26*(5), 1578–1591.
Rubenstein, M., Cornejo, A., & Nagpal, R. (2014). Programmable self-assembly in a thousand-robot swarm. *Science*, *345*(6198), 795–799.
Selivanov, A., & Fridman, E. (2022). PDE-based deployment of multiagents measuring relative position to one neighbor. *IEEE Control Systems Letters*, *6*, 2563–2568.
Tang, S.-X., Qi, J., & Zhang, J. (2017). Formation tracking control for multi-agent systems: A wave-equation based approach. *International Journal of Control, Automation and Systems*, *15*(6), 2704–2713.
Terushkin, M., & Fridman, E. (2021). Network-based deployment of nonlinear multi agents over open curves: A PDE approach. *Automatica*, *129*, Article 109697.
Vazquez, R., & Krstic, M. (2016a). Boundary control of a singular reaction-diffusion equation on a disk. *IFAC-PapersOnLine*, *49*(8), 74–79.
Vazquez, R., & Krstic, M. (2016b). Explicit output-feedback boundary control of reaction-diffusion PDEs on arbitrary-dimensional balls. *ESAIM: Control, Optimisation and Calculus of Variations*, *22*(4), 1078–1096.
Vazquez, R., & Krstic, M. (2019). Boundary control and estimation of reaction–diffusion equations on the sphere under revolution symmetry conditions. *International Journal of Control*, *92*(1), 2–11.
Vazquez, R., Krstic, M., Zhang, J., & Qi, J. (2019). Stabilization of a 2-D reaction-diffusion equation with a coupled PDE evolving on its boundary. In *2019 IEEE 58th conference on decision and control (CDC)* (pp. 2169–2174). IEEE.
Vazquez, R., Zhang, J., Qi, J., & Krstic, M. (2023). Kernel well-posedness and computation by power series in backstepping output feedback for radially-dependent reaction–diffusion PDEs on multidimensional balls. *Systems & Control Letters*, *177*, Article 105538.
Vicsek, T., & Zafeiris, A. (2012). Collective motion. *Physics Reports*, *517*(3–4), 71–140.
Wei, J., Fridman, E., & Johansson, K. H. (2019). A PDE approach to deployment of mobile agents under leader relative position measurements. *Automatica*, *106*, 47–53.
Wu, H.-N., & Wang, H.-D. (2015). Distributed consensus observers-based H_∞ control of dissipative PDE systems using sensor networks. *IEEE Transactions on Control of Network Systems*, *2*(2), 112–121.
Yang, C., Huang, T., Zhang, A., Qiu, J., Cao, J., & Alsaadi, F. E. (2018). Output consensus of multiagent systems based on PDEs with input constraint: A boundary control approach. *IEEE Transactions on Systems, Man, and Cybernetics: Systems*, [ISSN: 2168-2216] *51*(1), 370–377.
Zavlanos, M. M., Tanner, H. G., Jadbabaie, A., & Pappas, G. J. (2009). Hybrid control for connectivity preserving flocking. *IEEE Transactions on Automatic Control*, *54*(12), 2869–2875.
Zhang, J., & Qi, J. (2021). Compensation of spatially-varying state delay for a first-order hyperbolic PIDE using boundary control. *Systems & Control Letters*, *157*, Article 105050.
Zhang, J., Qi, J., Dubljevic, S., & Shen, B. (2022). Output regulation for a first-order hyperbolic PIDE with state and sensor delays. *European Journal of Control*, *65*, Article 100643.
Zhang, J., Vazquez, R., Qi, J., & Krstic, M. (2019). Simulation movie of 3-D deployment. Website. https://www.dropbox.com/s/owdexn8ct3v8zss/deployment.mp4?dl=0.
Zhao, Y., Duan, Q., Wen, G., Zhang, D., & Wang, B. (2018). Time-varying formation for general linear multiagent systems over directed topologies: A fully distributed adaptive technique. *IEEE Transactions on Systems, Man, and Cybernetics: Systems*, *51*(1), 532–541.
Zheng, Y., Zhao, Q., Ma, J., & Wang, L. (2019). Second-order consensus of hybrid multi-agent systems. *Systems & Control Letters*, *125*, 51–58.

Jing Zhang received her Ph.D. degree and M.S. degree in Control Science and Control Engineering from Donghua University and the B.S. degree in Automation from Shanxi University. She is currently a lecturer at the College of Information Engineering at Shanghai Maritime University, China. She has been a visiting student with the Aerospace Engineering Department, University of Seville, Spain from 2018 to 2019. Her research interests include the control and estimation of distributed parameter systems and the cooperative control of multi-agent system.

Rafael Vazquez received the electrical engineering and mathematics degrees from the University of Seville, Seville, Spain, and the M.Sc. and Ph.D. degrees in aerospace engineering from the University of California, San Diego. He is currently Professor in the Aerospace Engineering Department of the University of Seville, Spain. His research interests include control theory, estimation and optimization, with applications to distributed parameter systems, spacecraft and aircraft guidance, navigation and control, and space surveillance and awareness. He is coauthor of more than 150 journal and conference publications and the book Control of Turbulent and Magnetohydrodynamic Channel Flows (Basel, Switzerland: Birkhauser, 2007). Dr. Vazquez currently serves as Associate Editor for Automatica and IEEE Control Systems Letters (L-CSS).

Jie Qi is Professor of Automation Department at the Donghua University, China. She received her Ph.D. degree in Systems Engineering (2005) and the B.S. degree in Automation (2000) from Northeastern University in Shenyang, China. She has been a visiting researcher with the Cymer Center for Control Systems and Dynamics at the University of California, San Diego, from March 2013 to February 2014 and from June to September in 2015; and a visiting researcher with the Chemical and Materials Engineering Department at the University of Alberta, from January 2019 to January 2020. Her research interests include control and estimation of distributed parameters systems, control of delayed systems, learning-based control and their applications in multiagent systems, traffic systems and fiber melt spinning processes. She currently serves as Associate Editor for Systems & Control Letters.

Miroslav Krstic is Distinguished Professor of Mechanical and Aerospace Engineering, holds the Alspach endowed chair, and is the founding director of the Cymer Center for Control Systems and Dynamics at UC San Diego. He also serves as Senior Associate Vice Chancellor for Research at UCSD. As a graduate student, Krstic won the UC Santa Barbara best dissertation award and student best paper awards at CDC and ACC. Krstic has been elected Fellow of seven scientific societies — IEEE, IFAC, ASME, SIAM, AAAS, IET (UK), and AIAA (Assoc. Fellow) – and as a foreign member of the Serbian Academy of Sciences and Arts and of the Academy of Engineering

of Serbia. He has received the Richard E. Bellman Control Heritage Award, SIAM Reid Prize, ASME Oldenburger Medal, Nyquist Lecture Prize, Paynter Outstanding Investigator Award, Ragazzini Education Award, IFAC Ruth Curtain Distributed Parameter Systems Award, IFAC Nonlinear Control Systems Award, Chestnut textbook prize, Control Systems Society Distinguished Member Award, the PECASE, NSF Career, and ONR Young Investigator awards, the Schuck ('96 and '19) and Axelby paper prizes, and the first UCSD Research Award given to an engineer. Krstic has also been awarded the Springer Visiting Professorship at UC Berkeley, the Distinguished Visiting Fellowship of the Royal Academy of Engineering, the Invitation Fellowship of the Japan Society for the Promotion of Science, and four honorary professorships outside of the United States. He serves as Editor-in-Chief of Systems & Control Letters and has been serving as Senior Editor in Automatica and IEEE Transactions on Automatic Control, as editor of two Springer book series, and has served as Vice President for Technical Activities of the IEEE Control Systems Society and as chair of the IEEE CSS Fellow Committee. Krstic has coauthored eighteen books on adaptive, nonlinear, and stochastic control, extremum seeking, control of PDE systems including turbulent flows, and control of delay systems.